A Two Variable Refined Plate Theory for Isogeometric Vibration Analysis of The Functionally Graded Piezoelectric Microplates with Porosities

P. T. HUNG[1,*], *P. PHUNG-VAN*[2]

[1]Faculty of Civil Engineering, Ho Chi Minh City University of Technology and Education, Ho Chi Minh City, Vietnam
[2]Faculty of Civil Engineering, HUTECH University, Ho Chi Minh City, Vietnam

*Corresponding Author: P. T. HUNG (Email: hungpht@hcmute.edu.vn)
(Received: 13-Nov-2022; accepted: 9-Dec-2022; published: 31-Dec-2022)
DOI: http://dx.doi.org/10.55579/jaec.202264.393

Abstract. *In this article, a free vibration analysis of the functionally graded porous piezoelectric (FGPP) microplates is firstly solved by using a combination of two variable refined plate theory (RPT), modified strain gradient theory (MSGT) and isogeometric analysis (IGA). The FGPP microplate is composed of piezoelectric material with pores, which are distributed across the plate thickness in uniform and non-uniform distributions. The modified strain gradient theory is used to capture the size effect on the natural frequency of the FGPP microplates. According to the variational principle of RPT with two variables, the governing equations are derived and solved by the IGA. The influence of the length scale parameters (LSPs), external electric voltage, power law index, length-to-thickness ratio, aspect ratio and boundary conditions (BCs) on the natural frequency of the FGPP microplates is studied. The numerical results show that a rise in the porosity coefficient makes a decrease in the microplate's stiffness, while an increase in LSPs leads to a rise in the microplate's stiffness.*

Keywords

Functionally graded porous piezoelectric microplate, isogemoetric analysis, free vibration, refined plate theory, modified strain gradient theory.

1. Introduction

The piezoelectric material can convert electrical energy into mechanical energy and vice versa. This material is used in the manufacture of sensors and actuators in control systems. Therefore, piezoelectric materials have attracted the attention of many engineers and scientists. Many studies on the mechanical behaviours of piezoelectric structures have been carried out in recent years. Specifically, Huang et al. [1] investigated the nonlinear vibration and dynamic response analyses of the laminated composite plate with functionally graded (FG) layer and piezoelectric layers in a thermal environment based on the higher-order shear deformation plate theory (HSDT) and general von Karman-type equation. The analytical nonlinear vibration of the sandwich FG circular plate with piezoelectric layers in a thermal environment was presented by Ebrahimi et al. [2]. Besides, Yang et al. [3] used the Kirchhoff plate

theory (KPT) to calculate the free vibration and buckling of the piezoelectric nanoplates under the external electric voltage based on the analytical method. The vibration and dynamic responses of the FG circular plates with two piezoelectric actuators in a thermal environment by using the analytical method were found in [4]. According to the differential quadrature method (DQM), Arani et al. [5] presented the nonlinear transverse vibration of the piezoelectric plate reinforced with single-walled carbon nanotubes (SWCNTs). In addition, Duc et al. [6] investigated the analytical nonlinear dynamic response and vibration of the FG piezoelectric plates reinforced by eccentrically outside stiffeners resting on an elastic foundation and in a thermal environment based on the first-order shear deformation theory (FSDT). Ellali et al. [7] found Navier's solution for the buckling response of the electro-magneto-elastic plates resting on an elastic foundation based on the third-order shear deformation theory (TSDT). On the order hand, according to the various plate theory, Tanzadeh et al. [8] presented the buckling and vibration of the piezoelectric laminated composite plate based on the finite strip method. Based on the finite element method and Euler-Bernoulli beam theory, El Harti et al. [9] used the analytical method to study the active vibration control of the FG beams with piezoelectric sensors and actuators. Liu et al. [10] proposed the IGA and the simple FSDT with four variables to present the active shape and vibration control of the FG plates with piezoelectric layers in a thermal environment. Recently, Phuc et al. [11] studied the free and forced vibration of functionally graded piezoelectric (FGP) plates in a thermal environment and resting on an elastic foundation according to the TSDT and FEM. Ahmed et al. [12] used the nonlocal higher-order plate theory to study the dynamic response of the FG porous piezoelectric nanoplate in a thermal environment based on the DQM. According to the modified couple stress theory and FSDT, the force and free vibration of the sandwich microplates with epoxy reinforced with graphene platelets core and two piezoelectric layers under external electric voltage were investigated by Abbaspour et al. [13]. Based on KPT and DQM, Wang et al. [14] researched the static bending and free vibration of FGP plates resting on an elastic foundation.

The modified strain gradient theory with three length-scale parameters was proposed by Lam et al. [15]. According to the MSGT and Timoshenko beam theory, Li and Feng [16] study microstructure-dependent static bending and free vibration of the piezoelectric beam under the transverse mechanic load and external electric voltage. Mohammadi et al. [17] used the KPT to investigate the buckling of the rectangular plate based on the MSGT. Besides, the modified strain gradient theory was derived in general curvilinear coordinates and performed by Ashoori and Mahmoodi [18]. According to the KPT, Hosseini et al. [19] presented the analytical biaxial buckling of the orthotropic multi-microplate system resting in the Pasternak foundation using MSGT. Based on the Euler-Bernoulli beam theory combined with FEM, Kandaz et al. [20] studied the bending of the gold microbeam according to the MSGT and MCST. Besides, Karamanli et al. [21] employed the quasi-3D theory and MSGT to present the size-dependent free vibration of the FG porous microbeams.

The isogeometric method was first proposed by Hughes et al. [22]. After that, many researchers used IGA to investigate the mechanical behaviours of the structures. For instance, Bazilevs et al. [23] employed the IGA to analyze wind turbines and turbomachinery. Takizawa et al. [24, 25] studied the computational problem of cardiovascular medicine and flow analysis according to the IGA, respectively. In addition, flow computations by using the mesh moving methods like the space–time and arbitrary Lagrangian–Eulerian methods were introduced in [26]. On the other hand, the size-dependent free vibration, bending and buckling of the microplates based on the MSGT and IGA can be found in Refs. [27, 28, 29]. Furthermore, the computational cost of IGA was also clearly discussed and investigated in Ref. [22]. To the best author's knowledge, there is no investigation using the MSGT and RPT with two variables to study the free vibration of the FGPP microplates under external electric voltage. Therefore, in this article, we employ the RPT with two variables and MSGT to present the free vibra-

tion of the FGPP microplates under the external electric voltage. The influence of the MLSPs, types of porous distributions, porosity distributions and geometrical parameters on the natural frequency of the FGP porous microplates are presented and discussed.

2. The Basic Equations

2.1. Material properties of the FGPP microplates

Let us consider the FGPP rectangular and circular microplates with the thickness h, as seen in Fig. 1. The pores are distributed across the plate thickness in uniform and non-uniform porous distributions. The material properties of the uniform porous and non-uniform porous distributions are formulated as [12]

$$Uniform: \begin{cases} c_{ij} = c_{ij_1}(1 - e_0\xi) \\ \rho = \rho_1(1 - e_m\xi) \\ e_{ij} = e_{ij1}(1 - e_0\xi) \\ k_{ij} = k_{ij1}(1 - e_0\xi) \\ \xi = \frac{1}{e_0} - \frac{1}{e_0}\left(\frac{2}{\pi}\sqrt{1 - e_0} - \frac{2}{\pi} + 1\right)^2 \end{cases} \quad (1)$$

$$Non{-}uniform: \begin{cases} c_{ij} = c_{ij1}\left(1 - e_0\cos\left(\frac{\pi z}{h}\right)\right) \\ \rho = \rho_1\left(1 - e_m\cos\left(\frac{\pi z}{h}\right)\right) \\ e_{ij} = e_{ij1}\left(1 - e_0\cos\left(\frac{\pi z}{h}\right)\right) \\ d_{ij} = d_{ij1}\left(1 - e_0\cos\left(\frac{\pi z}{h}\right)\right) \end{cases}$$

where c_{ij} and ρ are stiffness coefficient and density, respectively; e_{ij} and d_{ij} are piezoelectric and dielectric constants. Index "1" indicates the maximum value of the material properties. Besides, e_0 and e_m are the porosity coefficient and porosity coefficient of density which are defined as follows

$$\begin{cases} e_0 = 1 - \frac{E_2}{E_1} = 1 - \frac{G_2}{G_1}, 0 < e_0 < 1 \\ e_m = 1 - \frac{\rho_2}{\rho_1}, 0 < e_m < 1 \end{cases} \quad (2)$$

in which E_1, G_1 and ρ_1 are the maximum Young modulus, shear modulus and density, respectively; E_2, G_2 and ρ_2 are the minimum Young modulus, shear modulus and density, respectively.

2.2. The refined plate theory with two variables

According to the RPT with two variables [30], the displacement fields at any point of the FGPP microplate are presented as follows

$$\mathbf{u} = \mathbf{u}_1 + z\mathbf{u}_2 + f(z)\mathbf{u}_3;$$

$$\mathbf{u}_1 = \begin{Bmatrix} 0 \\ 0 \\ w_b + w_s \end{Bmatrix};$$

$$\mathbf{u}_2 = \begin{Bmatrix} -w_{b,x} \\ -W_{b,y} \\ 0 \end{Bmatrix}; \quad (3)$$

$$\mathbf{u}_3 = \begin{Bmatrix} w_{s,x} \\ w_{s,y} \\ 0 \end{Bmatrix};$$

where w_b and w_s are bending and shear deflections along the z-directions, respectively. Index "," stands for the differential operator; $f(z) = -\frac{4z^3}{3h^2}$ is the distribution function.

According to the displacement fields in Eq. (3), the linear strain tensor is presented as

$$\boldsymbol{\varepsilon} = \begin{Bmatrix} \boldsymbol{\varepsilon}_b \\ \boldsymbol{\varepsilon}_s \end{Bmatrix} = \begin{Bmatrix} z\boldsymbol{\varepsilon}_{b1} + f(z)\boldsymbol{\varepsilon}_{b2} \\ (1 + f'(z))\boldsymbol{\gamma}_s \end{Bmatrix} \quad (4)$$

where

$$\boldsymbol{\varepsilon}_{b1} = -\begin{Bmatrix} w_{b,xx} \\ w_{b,yy} \\ 2w_{b,xy} \end{Bmatrix};$$

$$\boldsymbol{\varepsilon}_{b2} = \begin{Bmatrix} w_{s,xx} \\ w_{s,yy} \\ 2w_{s,xy} \end{Bmatrix}; \quad (5)$$

$$\boldsymbol{\gamma}_s = \begin{Bmatrix} w_{s,x} \\ w_{s,y} \end{Bmatrix}.$$

The electric potential can be assumed to contain cosine and linear variation across the plate thickness to fulfill Maxwell's equation as follows [31]

$$\Phi(x, y, z) = g(z)\phi(x, y) + \frac{2z}{h}V_0 \quad (6)$$

where Φ is the electric potential; V_0 is the initial electric voltage. Also, $g(z) = -cos(\frac{\pi z}{h})$ is a distributed function.

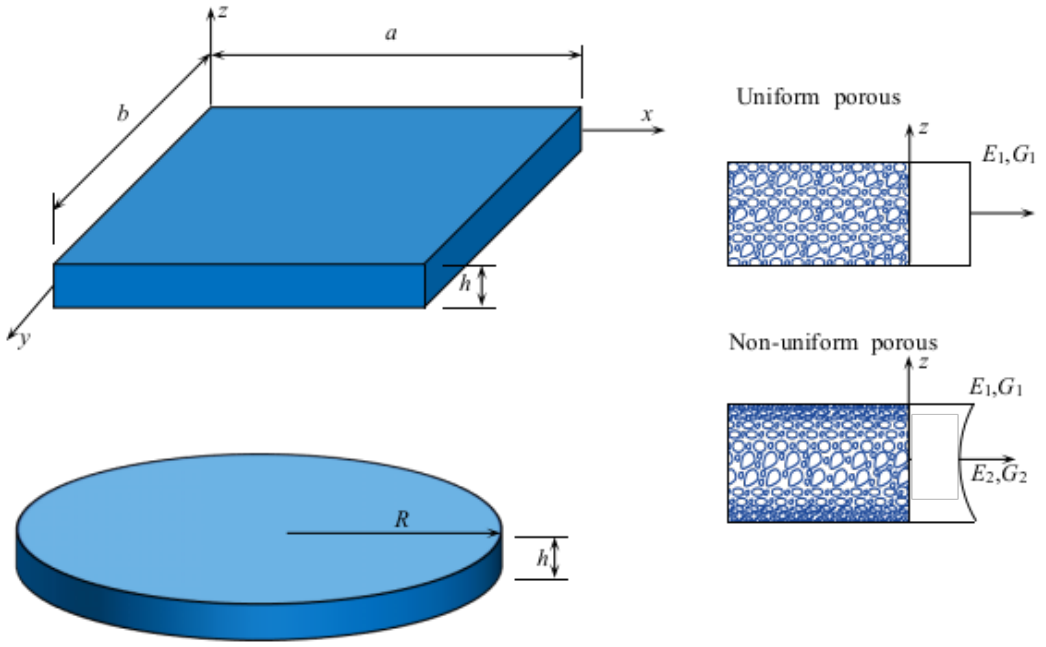

Fig. 1: The geometry of the FGPP rectangular and circular microplates.

Based on Maxwell's equation, the electric field can be derived from Eq. (6) by

$$\mathbf{E} = -\Delta\Phi$$

or

$$\begin{Bmatrix} E_x \\ E_y \\ E_z \end{Bmatrix} = -\begin{Bmatrix} \Phi_x \\ \Phi_y \\ \Phi_z \end{Bmatrix} = -\begin{Bmatrix} g(z)\phi_{,x} \\ g(z)\phi_{,x} \\ g'(z)\phi + \frac{2V_0}{h} \end{Bmatrix} \quad (7)$$

where E_x, E_y, E_z are the components of the electric field.

The rotation gradient tensor of the plate based on the displacement fields in Eq. (3) is expressed by

$$\begin{aligned} \boldsymbol{\chi} = \frac{1}{2}\left(\nabla\boldsymbol{\theta} + \nabla\boldsymbol{\theta}^T\right) &= \begin{Bmatrix} \boldsymbol{\chi}_b \\ \boldsymbol{\chi}_s \end{Bmatrix} \\ &= \begin{Bmatrix} \boldsymbol{\chi}_{1b} + f'(z)\,\boldsymbol{\chi}_{2b} \\ f''(z)\,\boldsymbol{\chi}_{1s} \end{Bmatrix} \end{aligned} \quad (8)$$

where

$$\boldsymbol{\theta} = \frac{1}{2}\left(\nabla\mathbf{u} - \nabla\mathbf{u}^T\right);$$

$$\boldsymbol{\chi}_b = \begin{Bmatrix} \chi_{xx} & \chi_{yy} & \boldsymbol{\chi}_{xy} \end{Bmatrix}^T; \boldsymbol{\chi}_s = \begin{Bmatrix} \chi_{xz} & \chi_{yz} \end{Bmatrix}^T; \quad (9)$$

$$\boldsymbol{\chi}_{1b} = \frac{1}{4}\begin{Bmatrix} 4w_{b,xy} + 2w_{s,xy} \\ -4w_{b,xy} - 2w_{s,xy} \\ 2\left(w_{b,yy} - w_{b,xx}\right) + \left(w_{x,yy} - w_{s,xx}\right) \end{Bmatrix};$$

$$\boldsymbol{\chi}_{2b} = \frac{1}{4}\begin{Bmatrix} -2w_{s,xy} \\ 2w_{s,xy} \\ w_{s,xx} - w_{s,yy} \end{Bmatrix}; \boldsymbol{\chi}_{1s} = \frac{1}{4}\begin{Bmatrix} -w_{s,y} \\ w_{s,x} \end{Bmatrix}$$

Similarly, the dilatation gradient tensor according to Eq. (3) takes the forms

$$\boldsymbol{\zeta} = \begin{Bmatrix} \zeta_x \\ \zeta_y \\ \zeta_z \end{Bmatrix} = \begin{Bmatrix} \varepsilon_{xx,x} + \varepsilon_{yy,x} + \varepsilon_{zz,x} \\ \varepsilon_{xx,y} + \varepsilon_{yy,y} + \varepsilon_{zz,y} \\ \varepsilon_{xx,z} + \varepsilon_{yy,z} + \varepsilon_{zz,z} \end{Bmatrix} = \ldots$$
$$\boldsymbol{\zeta}_1 + z\boldsymbol{\zeta}_2 + f(z)\,\boldsymbol{\zeta}_3 + f'(z)\,\boldsymbol{\zeta}_4 \quad (10)$$

where

$$\boldsymbol{\zeta}_1 = \begin{Bmatrix} 0 \\ 0 \\ -w_{b,xx} - w_{b,yy} \end{Bmatrix};$$
$$\boldsymbol{\zeta}_2 = -\begin{Bmatrix} w_{b,xxx} + w_{b,xyy} \\ w_{b,yyy} + w_{b,xxy} \\ 0 \end{Bmatrix};$$
$$\boldsymbol{\zeta}_3 = \begin{Bmatrix} w_{s,xxx} + w_{s,xyy} \\ w_{s,yyy} + w_{s,xxy} \\ 0 \end{Bmatrix}; \quad (11)$$
$$\boldsymbol{\zeta}_4 = \begin{Bmatrix} 0 \\ 0 \\ w_{s,xx} + w_{s,yy} \end{Bmatrix}.$$

In addition, the deviatoric stretch gradient tensor is expressed as follows

$$\boldsymbol{\eta} = \begin{Bmatrix} \boldsymbol{\eta}_b \\ \boldsymbol{\eta}_s \end{Bmatrix} = \begin{Bmatrix} z\boldsymbol{\eta}_{b1} + f(z)\,\boldsymbol{\eta}_{b2} + f''(z)\,\boldsymbol{\eta}_{b3} \\ \boldsymbol{\eta}_{s1} + f'(z)\,\eta_{s2} \end{Bmatrix} \quad (12)$$

where

$$\boldsymbol{\eta}_b = \begin{Bmatrix} \eta_{xxx} & \eta_{yyy} & \eta_{yyx} & \eta_{xxy} & \eta_{zzx} & \eta_{zzy} \end{Bmatrix}^T;$$
$$\boldsymbol{\eta}_s = \begin{Bmatrix} \eta_{zzz} & \eta_{xxz} & \eta_{yyz} & \eta_{xyz} \end{Bmatrix}^T;$$
$$\eta_{ijk} = \frac{1}{3}\left(\varepsilon_{ij,k} + \varepsilon_{jk,i} + \varepsilon_{ik,j}\right) - ...$$
$$\frac{1}{15}(\delta_{ij}\left(\varepsilon_{mm,k} + 2\varepsilon_{mk,m}\right) + ...$$
$$\delta_{ik}\left(\varepsilon_{mm,j} + 2\varepsilon_{mj,m}\right)) - ...$$
$$\frac{1}{15}\left(\delta_{jk}\left(\varepsilon_{mm,i} + 2\varepsilon_{mi,m}\right)\right); \quad (13)$$

$$\boldsymbol{\eta}_{b1} = \frac{1}{5}\begin{Bmatrix} -2w_{b,xxx} + 3w_{b,xyy} \\ -2w_{b,yyy} + 3w_{b,xxy} \\ w_{b,xxx} - 4w_{b,xyy} \\ w_{b,yyy} - 4w_{b,xxy} \\ w_{b,xxx} + w_{b,xyy} \\ w_{b,yyy} + w_{b,xxy} \end{Bmatrix};$$
$$\boldsymbol{\eta}_{b2} = \frac{1}{5}\begin{Bmatrix} 2w_{s,xxx} - 3w_{s,xyy} \\ 2w_{s,yyy} - 3w_{s,xxy} \\ -w_{s,xxx} + 4w_{s,xyy} \\ -w_{s,yyy} + 4w_{s,xxy} \\ -w_{s,xxx} - w_{s,xyy} \\ -w_{s,yyy} - w_{s,xxy} \end{Bmatrix};$$
$$\boldsymbol{\eta}_{b3} = \frac{1}{15}\begin{Bmatrix} -3w_{s,x} \\ -3w_{s,y} \\ -w_{s,x} \\ -w_{s,y} \\ 4w_{s,x} \\ 4w_{s,y} \end{Bmatrix};$$
$$\boldsymbol{\eta}_{s1} = \tfrac{1}{15}\begin{Bmatrix} 3w_{b,xx} + 3w_{b,yy} - 3w_{s,xx} - 3w_{s,yy} \\ -4w_{b,xx} + w_{b,yy} + 4w_{s,xx} - w_{s,yy} \\ -4w_{b,yy} + w_{b,xx} + 4w_{s,yy} - w_{s,xx} \\ -5w_{b,xy} + 5w_{s,xy} \end{Bmatrix};$$
$$\boldsymbol{\eta}_{s2} = \frac{1}{15}\begin{Bmatrix} -6w_{s,xx} - 6w_{s,yy} \\ 8w_{s,xx} - 2w_{s,yy} \\ 8w_{s,yy} - 2w_{s,xx} \\ 10w_{s,xy} \end{Bmatrix};$$

in which, δ denotes the Kronecker's delta.

The constitutive equations of the FGPP microplates employing the MSGT [15] can be presented as follows

$$\begin{Bmatrix} \sigma_x \\ \sigma_y \\ \widehat{\tau}_{xy} \\ \widehat{\tau}_{xz} \\ \widehat{\tau}_{yz} \end{Bmatrix} = \begin{bmatrix} \bar{c}_{11} & \bar{c}_{12} & 0 & 0 & 0 \\ \bar{c}_{12} & \bar{c}_{22} & 0 & 0 & 0 \\ 0 & 0 & \bar{c}_{66} & 0 & 0 \\ 0 & 0 & 0 & \bar{c}_{44} & 0 \\ 0 & 0 & 0 & 0 & \bar{c}_{55} \end{bmatrix} \begin{Bmatrix} \varepsilon_x \\ \varepsilon_y \\ \gamma_{xy} \\ \gamma_{xz} \\ \gamma_{yz} \end{Bmatrix} - ...$$
$$\begin{bmatrix} 0 & 0 & \bar{e}_{31} \\ 0 & 0 & \bar{e}_{31} \\ 0 & 0 & 0 \\ \bar{e}_{15} & 0 & 0 \\ 0 & \bar{e}_{15} & 0 \end{bmatrix} \begin{Bmatrix} E_x \\ E_y \\ E_z \end{Bmatrix};$$
$$\begin{Bmatrix} D_x \\ D_y \\ D_z \end{Bmatrix} = \begin{Bmatrix} 0 & 0 & 0 & \bar{e}_{15} & 0 \\ 0 & 0 & 0 & 0 & \bar{e}_{15} \\ \bar{e}_{31} & \bar{e}_{31} & 0 & 0 & 0 \end{Bmatrix} \begin{Bmatrix} \varepsilon_x \\ \varepsilon_y \\ \gamma_{xy} \\ \gamma_{xz} \\ \gamma_{yz} \end{Bmatrix} + ... \quad (14)$$
$$\begin{bmatrix} \bar{k}_{11} & 0 & 0 \\ 0 & \bar{k}_{22} & 0 \\ 0 & 0 & \bar{k}_{33} \end{bmatrix} \begin{Bmatrix} E_x \\ E_y \\ E_z \end{Bmatrix};$$
$$\begin{Bmatrix} m_{xx} \\ m_{yy} \\ m_{xy} \\ m_{xz} \\ m_{yz} \end{Bmatrix} = 2\mu {l_1}^2 \begin{bmatrix} 1 & 0 & 0 & 0 & 0 \\ 0 & 1 & 0 & 0 & 0 \\ 0 & 0 & 1 & 0 & 0 \\ 0 & 0 & 0 & 1 & 0 \\ 0 & 0 & 0 & 0 & 1 \end{bmatrix} \begin{Bmatrix} \chi_{xx} \\ \chi_{yy} \\ \chi_{xy} \\ \chi_{xz} \\ \chi_{yz} \end{Bmatrix};$$
$$\begin{Bmatrix} p_x \\ p_y \\ p_z \end{Bmatrix} = 2\mu l_2^2 \begin{bmatrix} 1 & 0 & 0 \\ 0 & 1 & 0 \\ 0 & 0 & 1 \end{bmatrix} \begin{Bmatrix} \zeta_x \\ \zeta_y \\ \zeta_z \end{Bmatrix};$$
$$\begin{Bmatrix} \tau_{xxx} \\ \tau_{yyy} \\ \tau_{yyx} \\ \tau_{xxy} \\ \tau_{zzx} \\ \tau_{zzy} \end{Bmatrix} = 2\mu {l_3}^2 \begin{bmatrix} 1 & 0 & 0 & 0 & 0 & 0 \\ 0 & 1 & 0 & 0 & 0 & 0 \\ 0 & 0 & 1 & 0 & 0 & 0 \\ 0 & 0 & 0 & 1 & 0 & 0 \\ 0 & 0 & 0 & 0 & 1 & 0 \\ 0 & 0 & 0 & 0 & 0 & 1 \end{bmatrix} \begin{Bmatrix} \eta_{xxx} \\ \eta_{yyy} \\ \eta_{yyx} \\ \eta_{xxy} \\ \eta_{zzx} \\ \eta_{zzy} \end{Bmatrix};$$

where $\sigma_x, \sigma_y, \widehat{\tau}_{xy}, \widehat{\tau}_{xz}, \widehat{\tau}_{yz}$ are the stress components; D_x, D_y, D_z are electric displacements;

m_{ij}, p_i and τ_{ijk} are the components of the higher stress tensor; l_1, l_2, l_3 are three LSPs; is Lame's coefficient. Furthermore, $\bar{c}_{ij}$, $\bar{e}_{ij}$ and $\bar{k}_{ij}$ are the reduced elastic coefficients, piezo-electric constants and dielectric coefficients, respectively, are defined as following

$$\begin{aligned}
&\bar{c}_{11} = c_{11} - \frac{c_{13}^2}{c_{33}};\ \bar{c}_{12} = c_{12} - \frac{c_{13}^2}{c_{33}};\\
&\bar{c}_{66} = c_{66};\ \bar{c}_{55} = c_{55};\ \bar{c}_{44} = c_{44};\\
&\bar{e}_{31} = e_{31} - \frac{e_{33}c_{13}}{c_{33}};\ \bar{e}_{15} = e_{15};\\
&\bar{k}_{33} = k_{33} + \frac{e_{33}^2}{c_{33}};\ \bar{k}_{11} = k_{11}
\end{aligned} \tag{15}$$

The constitutive equations (14) in matrix form is rewritten as follows

$$\begin{cases}
\boldsymbol{\sigma}_b = \mathbf{C}_{ub}\boldsymbol{\varepsilon}_b - \mathbf{C}_{ueb}\mathbf{E}_b;\\
\boldsymbol{\sigma}_s = \mathbf{C}_{us}\boldsymbol{\varepsilon}_s - \mathbf{C}_{ues}\mathbf{E}_s;\\
\mathbf{D}_b = \mathbf{C}_{ueb}^T\boldsymbol{\varepsilon}_b + \mathbf{C}_{eeb}\mathbf{E}_b;\\
\mathbf{D}_s = \mathbf{C}_{ues}^T\boldsymbol{\varepsilon}_s + \mathbf{C}_{ees}\mathbf{E}_s;\\
\mathbf{m}_b = 2\mu l_1^2\mathbf{I}_{3\times3}\boldsymbol{\chi}_b;\\
\mathbf{m}_s = 2\mu l_1^2\mathbf{I}_{2\times2}\boldsymbol{\chi}_s;\\
\mathbf{p} = 2\mu l_2^2\mathbf{I}_{3\times3}\boldsymbol{\zeta};\\
\boldsymbol{\tau}_b = 2\mu l_3^2\mathbf{I}_{6\times6}\boldsymbol{\eta}_b;\\
\boldsymbol{\tau}_s = 2\mu l_3^2\mathbf{I}_{4\times4}\boldsymbol{\eta}_s
\end{cases} \tag{16}$$

where

$$\begin{aligned}
&\boldsymbol{\sigma}_b = \begin{Bmatrix}\sigma_x & \sigma_y & \widehat{\tau}_{xy}\end{Bmatrix}^T;\\
&\boldsymbol{\sigma}_s = \begin{Bmatrix}\widehat{\tau}_{xz} & \widehat{\tau}_{yz}\end{Bmatrix}^T;\\
&\mathbf{D}_b = \begin{Bmatrix}0 & 0 & D_z\end{Bmatrix}^T;\\
&\mathbf{D}_s = \begin{Bmatrix}D_x & D_y\end{Bmatrix}^T;\\
&\mathbf{E}_b = \begin{Bmatrix}0 & 0 & E_z\end{Bmatrix}^T;\\
&\mathbf{E}_s = \begin{Bmatrix}E_x & E_y\end{Bmatrix}^T;\\
&\mathbf{m}_b = \begin{Bmatrix}m_{xx} & m_{yy} & m_{xy}\end{Bmatrix}^T;\\
&\mathbf{m}_s = \begin{Bmatrix}m_{xz} & m_{yz}\end{Bmatrix}^T;\\
&\mathbf{p} = \begin{Bmatrix}p_x & p_y & p_z\end{Bmatrix}^T;\\
&\boldsymbol{\tau}_b = \begin{Bmatrix}\tau_{xxx} & \tau_{yyy} & \tau_{yyx} & \tau_{xxy} & \tau_{zzx} & \tau_{zzy}\end{Bmatrix}^T;\\
&\boldsymbol{\tau}_s = \begin{Bmatrix}\tau_{zzz} & \tau_{xxz} & \tau_{yyz} & \tau_{xyz}\end{Bmatrix}^T;\\
&\mathbf{C}_{ub} = \begin{bmatrix}\bar{c}_{11} & \bar{c}_{12} & 0\\ \bar{c}_{12} & \bar{c}_{22} & 0\\ 0 & 0 & \bar{c}_{66}\end{bmatrix};\ \mathbf{C}_{us} = \begin{bmatrix}\bar{c}_{55} & 0\\ 0 & \bar{c}_{44}\end{bmatrix};\\
&\mathbf{C}_{ues} = \begin{bmatrix}\bar{e}_{15} & 0\\ 0 & \bar{e}_{15}\end{bmatrix};\ \mathbf{C}_{ees} = \begin{bmatrix}\bar{k}_{11} & 0\\ 0 & \bar{k}_{11}\end{bmatrix};\\
&\mathbf{C}_{ueb} = \begin{bmatrix}0 & 0 & \bar{e}_{31}\\ 0 & 0 & \bar{e}_{31}\\ 0 & 0 & 0\end{bmatrix};\ \mathbf{C}_{eeb} = \begin{bmatrix}0 & 0 & 0\\ 0 & 0 & 0\\ 0 & 0 & \bar{k}_{33}\end{bmatrix}
\end{aligned} \tag{17}$$

In addition, $\mathbf{m}$, $\mathbf{p}$ and $\boldsymbol{\tau}$ are the higher-order stress tensors; $\mathbf{I}_{2\times2}$, $\mathbf{I}_{3\times3}$, $\mathbf{I}_{4\times4}$, $\mathbf{I}_{6\times6}$ are the identity matrices of size of 2×2, 3×3, 4×4 and 6×6, respectively.

2.3. The Hamilton principle

Based on the Hamilton's principle, the governing equation of the FGPP microplates is expressed as follows

$$\int_0^t \Big(\delta\Pi + \delta K - \delta V\Big) = 0 \tag{18}$$

where $\delta\Pi$, δK and δV are the virtual strain energy, kinetic energy and work done by the external electric voltage, respectively.

The virtual strain energy of the FGPP MSGT microplate is defined as [15]

$$\delta\Pi = \int_V \begin{pmatrix}\delta\boldsymbol{\varepsilon}_b^T\boldsymbol{\sigma}_b + \delta\boldsymbol{\varepsilon}_s^T\boldsymbol{\sigma}_s - \delta\mathbf{E}_b^T\mathbf{D}_b - ...\\ \delta\mathbf{E}_s^T\mathbf{D}_s + \delta\boldsymbol{\chi}^T\mathbf{m} + \delta\boldsymbol{\zeta}^T\mathbf{p} + \delta\boldsymbol{\eta}^T\boldsymbol{\tau}\end{pmatrix} dV \tag{19}$$

The virtual kinetic energy is express as

$$\delta K = \int_{\Omega} \delta \bar{\mathbf{u}}^T \bar{\mathbf{m}} \ddot{\bar{\mathbf{u}}} \mathrm{d}\Omega \tag{20}$$

where

$$\bar{\mathbf{u}} = \begin{Bmatrix} \mathbf{u}_1 \\ \mathbf{u}_2 \\ \mathbf{u}_3 \end{Bmatrix}; \quad \bar{\mathbf{m}} = \begin{bmatrix} \mathbf{I}_0 & \mathbf{0} & \mathbf{0} \\ \mathbf{0} & \mathbf{I}_0 & \mathbf{0} \\ \mathbf{0} & \mathbf{0} & \mathbf{I}_0 \end{bmatrix}; \quad \mathbf{I}_0 = \begin{bmatrix} I_1 & I_2 & I_4 \\ I_2 & I_3 & I_5 \\ I_4 & I_5 & I_6 \end{bmatrix}; \tag{21}$$

$$(I_1, I_2, I_3, I_4, I_5, I_6) = ... \int_{-h/2}^{h/2} \rho(z) \left(1, z, z^2, f, zf, f^2\right) \mathrm{d}z$$

Besides, the virtual work done by the external electric load is taken by

$$\delta V = h \int_{\Omega} \delta \mathbf{N}_w^T \mathbf{N}_e \mathbf{N}_w \mathrm{d}\Omega \tag{22}$$

in which

$$\mathbf{N}_w = \begin{Bmatrix} w_{b,x} + w_{s,x} \\ w_{b,y} + w_{s,y} \end{Bmatrix}; \quad \mathbf{N}_e = \begin{bmatrix} -2\bar{e}_{31} V_0 & 0 \\ 0 & -2\bar{e}_{31} V_0 \end{bmatrix}. \tag{23}$$

Inserting the necessary equations into Eq. (18), the weak form of the equation of motion is re-formed as follows

$$\begin{aligned} &\int_{\Omega} \delta \bar{\boldsymbol{\varepsilon}}^{bT} \bar{\mathbf{D}}_{ub} \bar{\boldsymbol{\varepsilon}}^b \mathrm{d}\Omega + \int_{\Omega} \delta \boldsymbol{\gamma}^{sT} \mathbf{D}_{us} \boldsymbol{\gamma}^s \mathrm{d}\Omega - ... \\ &\int_{\Omega} \delta \boldsymbol{\gamma}^{sT} \bar{\mathbf{D}}_{ueb} \bar{\mathbf{E}}^b \mathrm{d}\Omega - \int_{\Omega} \delta \boldsymbol{\gamma}^{sT} \bar{\mathbf{D}}_{ues} \bar{\mathbf{E}}^s \mathrm{d}\Omega - ... \\ &\int_{\Omega} \delta \bar{\mathbf{E}}^{bT} \bar{\mathbf{D}}_{ueb}^T \bar{\boldsymbol{\varepsilon}}^b \mathrm{d}\Omega - \int_{\Omega} \delta \bar{\mathbf{E}}^{sT} \bar{\mathbf{D}}_{ues}^T \boldsymbol{\gamma}^s \mathrm{d}\Omega - ... \\ &\int_{\Omega} \delta \bar{\mathbf{E}}^{bT} \bar{\mathbf{D}}_{eeb} \bar{\mathbf{E}}^b \mathrm{d}\Omega - \int_{\Omega} \delta \bar{\mathbf{E}}^{sT} \bar{\mathbf{D}}_{ees} \bar{\mathbf{E}}^s \mathrm{d}\Omega + ... \\ &\int_{\Omega} \delta \bar{\boldsymbol{\chi}}^{bT} \bar{\mathbf{D}}_r^b \bar{\boldsymbol{\Gamma}}_r^b \bar{\boldsymbol{\chi}}^b \mathrm{d}\Omega + \int_{\Omega} \delta \boldsymbol{\chi}^{sT} \bar{\mathbf{D}}_r^s \bar{\boldsymbol{\Gamma}}_r^s \boldsymbol{\chi}^s \mathrm{d}\Omega + ... \\ &\int_{\Omega} \delta \bar{\boldsymbol{\zeta}}^T \bar{\mathbf{D}}^{dil} \bar{\boldsymbol{\zeta}} \mathrm{d}\Omega + \int_{\Omega} \delta \bar{\boldsymbol{\eta}}^{bT} \bar{\mathbf{D}}^{deb} \bar{\boldsymbol{\Gamma}}^{deb} \bar{\boldsymbol{\eta}}^b \mathrm{d}\Omega + ... \\ &\int_{\Omega} \delta \bar{\boldsymbol{\eta}}^{sT} \bar{D}^{des} \bar{\boldsymbol{\Gamma}}^{des} \bar{\boldsymbol{\eta}}^s \mathrm{d}\Omega + \int_{\Omega} \delta \bar{\mathbf{u}}^T \bar{\mathbf{m}} \ddot{\bar{\mathbf{u}}} \mathrm{d}\Omega - ... \\ &h \int_{\Omega} \delta \mathbf{N}_w^T \mathbf{N}_e \mathbf{N}_w \mathrm{d}\Omega = \mathbf{0} \end{aligned} \tag{24}$$

where

$$\begin{aligned} &\bar{\mathbf{D}}_{ub} = \begin{bmatrix} \mathbf{A}_b & \mathbf{B}_b \\ \mathbf{B}_b & \mathbf{D}_b \end{bmatrix}; \; \bar{\mathbf{D}}_{rb} = \begin{bmatrix} \mathbf{A}_{rb} & \mathbf{B}_{rb} \\ \mathbf{B}_{rb} & \mathbf{D}_{rb} \end{bmatrix}; \\ &(\mathbf{A}_b, \mathbf{B}_b, \mathbf{D}_b) = \int_{-h/2}^{h/2} \left(z^2, zf, f^2\right) \mathbf{C}_{ub} \mathrm{d}z; \\ &(\mathbf{A}_{rb}, \mathbf{B}_{rb}, \mathbf{D}_{rb}) = \textstyle\int_{-h/2}^{h/2} 2\mu {l_1}^2 \left(1, f', f'^2\right) \mathbf{I}_{3x3} \mathrm{d}z; \\ &(\mathbf{A}_{rs}, \mathbf{B}_{rs}, \mathbf{D}_{rs}) = \textstyle\int_{-h/2}^{h/2} 2\mu {l_1}^2 \left(1, f'', f''^2\right) \mathbf{I}_{2x2} \mathrm{d}z; \\ &\mathbf{D}_{us} = \int_{-h/2}^{h/2} (1 + f')^2 \mathbf{C}_u^s \mathrm{d}z; \\ &\bar{\mathbf{D}}_{ueb} = \left\{ \mathbf{C}_{ueb}^1 \quad \mathbf{C}_{ueb}^2 \right\}; \\ &\left(\mathbf{C}_{ueb}^1, \mathbf{C}_{ueb}^2\right) = -\int_{-h/2}^{h/2} \mathbf{C}_{ueb}(z, f) \, g' \mathrm{d}z; \\ &\bar{\mathbf{D}}_{ues} = -\int_{-h/2}^{h/2} \mathbf{C}_{ues} (1 + f') \, g \mathrm{d}z; \\ &\bar{\mathbf{D}}_{eeb} = \textstyle\int_{-h/2}^{h/2} \mathbf{C}_{eeb} g'^2 \mathrm{d}z; \; \bar{\mathbf{D}}_{ees} = \textstyle\int_{-h/2}^{h/2} \mathbf{C}_{ees} g^2 \mathrm{d}z; \end{aligned} \tag{25}$$

$$\bar{\mathbf{D}}_{di} = \begin{bmatrix} A_{di} & B_{di} & C_{di} & E_{di} \\ B_{di} & D_{di} & F_{di} & L_{di} \\ C_{di} & F_{di} & H_{di} & O_{di} \\ E_{di} & L_{di} & O_{di} & P_{di} \end{bmatrix};$$

$$\bar{\mathbf{D}}_{deb} = \begin{bmatrix} A_{deb} & B_{deb} & C_{deb} & E_{deb} \\ B_{deb} & D_{deb} & F_{deb} & L_{deb} \\ C_{deb} & F_{deb} & H_{deb} & O_{deb} \\ E_{deb} & L_{deb} & O_{deb} & P_{deb} \end{bmatrix};$$

$(\mathbf{A}_{di},\mathbf{B}_{di},\mathbf{D}_{di},\mathbf{C}_{di},\mathbf{E}_{di},\mathbf{F}_{di},\mathbf{L}_{di},\mathbf{H}_{di},\mathbf{O}_{di},\mathbf{P}_{di}) = ...$
$\int_{-h/2}^{h/2} 2\mu {l_2}^2 \left(1,z,z^2,f,f',zf,zf',f^2,ff',{f'}^2\right)\mathbf{I}_{3x3}\mathrm{d}z;$
$(\mathbf{A}_{deb},\mathbf{B}_{deb},\mathbf{D}_{deb},\mathbf{C}_{deb},\mathbf{E}_{deb},\mathbf{F}_{deb},\mathbf{L}_{deb},\mathbf{H}_{deb},\mathbf{O}_{deb},\mathbf{P}_{deb}) = ...$
$\int_{-h/2}^{h/2} 2\mu {l_3}^2 \left(1,z,z^2,f,f'',zf,zf'',f^2(z),ff'',{f''}^2\right)\mathbf{I}_{6x6}\mathrm{d}z;$

$$(\mathbf{A}_{des},\mathbf{B}_{des},\mathbf{D}_{des}) = \int_{-h/2}^{h/2} 2\mu {l_3}^2 \left(1,f',{f'}^2\right)\mathbf{I}_{4x4}\mathrm{d}z;$$

$$\bar{\mathbf{D}}_{rs} = \begin{bmatrix}\mathbf{A}_{rs} & \mathbf{B}_{rs}\\ \mathbf{B}_{rs} & \mathbf{D}_{rs}\end{bmatrix}; \bar{\mathbf{D}}_{des} = \begin{bmatrix}\mathbf{A}_{des} & \mathbf{B}_{des}\\ \mathbf{B}_{des} & \mathbf{D}_{des}\end{bmatrix};$$

$$\bar{\mathbf{\Gamma}}_{deb} = \begin{bmatrix}\mathbf{\Gamma}_{deb} & \mathbf{0} & \mathbf{0} & \mathbf{0}\\ \mathbf{0} & \mathbf{\Gamma}_{deb} & \mathbf{0} & \mathbf{0}\\ \mathbf{0} & \mathbf{0} & \mathbf{\Gamma}_{deb} & \mathbf{0}\\ \mathbf{0} & \mathbf{0} & \mathbf{0} & \mathbf{\Gamma}_{deb}\end{bmatrix};$$

$$\bar{\mathbf{\Gamma}}_{rb} = \begin{bmatrix}\mathbf{\Gamma}_{rb} & \mathbf{0}\\ \mathbf{0} & \mathbf{\Gamma}_{rb}\end{bmatrix}; \bar{\mathbf{\Gamma}}_{rs} = \begin{bmatrix}\mathbf{\Gamma}_{rs} & \mathbf{0}\\ \mathbf{0} & \mathbf{\Gamma}_{rs}\end{bmatrix}; \bar{\mathbf{\Gamma}}_{des} = \begin{bmatrix}\mathbf{\Gamma}_{des} & \mathbf{0}\\ \mathbf{0} & \mathbf{\Gamma}_{des}\end{bmatrix};$$
$$\mathbf{\Gamma}_{rb} = diag\,(1,1,2)\,;\ \mathbf{\Gamma}_{rs} = diag\,(2,2)\,;$$
$$\mathbf{\Gamma}_{deb} = diag\,(1,1,3,3,3,3)\,;\ \mathbf{\Gamma}_{des} = diag\,(1,3,3,6)$$

2.4. The isogeometric approximation

The displacement vector u according to the NURBS basic function [22] is approximated as follows

$$\mathbf{u}(x,y) = \sum_{I=1}^{m\times n} \mathbf{N}_I(x,y)\mathbf{q}_I \tag{26}$$

where

$$\mathbf{N}_I(x,y) = \begin{bmatrix}N_I(x,y) & 0 & 0\\ 0 & N_I(x,y) & 0\\ 0 & 0 & N_I(x,y)\end{bmatrix};$$
$$\mathbf{q}_I = \{w_{bI}, w_{sI}, \varphi_I\}^T \tag{27}$$

in which $N_I(x,y)$ is the NURBS basic function.

Substituting Eq. (26) into Eqs. (4), (8), (10) and (12), the strain, the rotation gradient, dilatation gradient, deviatoric stretch gradient tensors and electric fields can be rewritten as follows

$$\begin{aligned}
&\bar{\varepsilon}^b = \begin{Bmatrix}\bar{\varepsilon}_{b1}\\ \bar{\varepsilon}_{b2}\end{Bmatrix} = \sum_{I=1}^{m\times n}\begin{Bmatrix}\mathbf{B}_{b1I}\\ \mathbf{B}_{b2I}\end{Bmatrix}\mathbf{q}_I = \sum_{I=1}^{n}\bar{\mathbf{B}}_{bI}\mathbf{q}_I;\\
&\boldsymbol{\gamma}^s = \sum_{I=1}^{m\times n}\bar{\mathbf{B}}_{sI}\mathbf{d}_I;\ \bar{\mathbf{E}}^b = \sum_{I=1}^{m\times n}\bar{\mathbf{B}}_{ebI}\mathbf{q}_I; \bar{\mathbf{E}}^s = \sum_{I=1}^{m\times n}\bar{\mathbf{B}}_{esI}\mathbf{q}_I;\\
&\bar{\boldsymbol{\chi}}^b = \begin{Bmatrix}\boldsymbol{\chi}_1^b\\ \boldsymbol{\chi}_2^b\end{Bmatrix} = \sum_{I=1}^{m\times n}\begin{Bmatrix}\mathbf{B}_{rI}^{b1}\\ \mathbf{B}_{rI}^{b2}\end{Bmatrix}\mathbf{q}_I = \sum_{I=1}^{m\times n}\bar{\mathbf{B}}_{rbI}\mathbf{q}_I;\\
&\boldsymbol{\chi}^s = \sum_{I=1}^{m\times n}\bar{\mathbf{B}}_{rsI}\mathbf{q}_I;\\
&\bar{\boldsymbol{\eta}}^b = \begin{Bmatrix}\bar{\boldsymbol{\eta}}_1^b\\ \bar{\boldsymbol{\eta}}_2^b\\ \bar{\boldsymbol{\eta}}_3^b\end{Bmatrix} = \sum_{I=1}^{m\times n}\begin{Bmatrix}\mathbf{B}_{1I}^{deb}\\ \mathbf{B}_{2I}^{deb}\\ \mathbf{B}_{3I}^{deb}\end{Bmatrix}\mathbf{q}_I = \sum_{I=1}^{m\times n}\bar{\mathbf{B}}_{debI}\mathbf{q}_I;\\
&\bar{\boldsymbol{\eta}}^s = \begin{Bmatrix}\bar{\boldsymbol{\eta}}_1^s\\ \bar{\boldsymbol{\eta}}_2^s\end{Bmatrix} = \sum_{I=1}^{m\times n}\begin{Bmatrix}\mathbf{B}_{1I}^{des}\\ \mathbf{B}_{2I}^{des}\end{Bmatrix}\mathbf{q}_I = \sum_{I=1}^{m\times n}\bar{\mathbf{B}}_{desI}\mathbf{q}_I
\end{aligned} \tag{28}$$

in which

$$\begin{aligned}
&\bar{\mathbf{B}}_{sI} = \begin{bmatrix}0 & N_{I,x} & 0\\ 0 & N_{I,y} & 0\end{bmatrix};\ \bar{\mathbf{B}}_{ebI} = \begin{Bmatrix}0\\ 0\\ -N_I\end{Bmatrix};\\
&\bar{\mathbf{B}}_{esI} = \begin{Bmatrix}-N_{I,x}\\ -N_{I,y}\end{Bmatrix};\ \bar{\mathbf{B}}_{rsI} = \frac{1}{4}\begin{bmatrix}0 & -N_{I,y} & 0\\ 0 & N_{I,x} & 0\end{bmatrix};\\
&\mathbf{B}_{b1I} = -\begin{bmatrix}N_{I,xx} & 0 & 0\\ N_{I,yy} & 0 & 0\\ 2N_{I,xy} & 0 & 0\end{bmatrix};\ \mathbf{B}_{b2I} = \begin{bmatrix}0 & N_{I,xx} & 0\\ 0 & N_{I,yy} & 0\\ 0 & 2N_{I,xy} & 0\end{bmatrix};
\end{aligned} \tag{29}$$

$$\mathbf{B}_{1I}^{deb} = \frac{1}{5}\begin{bmatrix}-2N_{I,xxx}+3N_{I,xyy} & 0 & 0\\ -2N_{I,yyy}+3N_{I,xxy} & 0 & 0\\ N_{I,xxx}-4N_{I,xyy} & 0 & 0\\ N_{I,yyy}-4N_{I,xxy} & 0 & 0\\ N_{I,xxx}+N_{I,xyy} & 0 & 0\\ N_{I,yyy}+N_{I,xxy} & 0 & 0\end{bmatrix};$$

$$\mathbf{B}_{2I}^{deb} = \frac{1}{5}\begin{bmatrix}0 & 2N_{I,xxx}-3N_{I,xyy} & 0\\ 0 & 2N_{I,yyy}-3N_{I,xxy} & 0\\ 0 & -N_{I,xxx}+4N_{I,xyy} & 0\\ 0 & -N_{I,yyy}+4N_{I,xxy} & 0\\ 0 & -N_{I,xxx}-N_{I,xyy} & 0\\ 0 & -N_{I,yyy}-N_{I,xxy} & 0\end{bmatrix};$$

$$\mathbf{B}_{3I}^{deb} = \frac{1}{15}\begin{bmatrix}0 & -3N_{I,x} & 0\\ 0 & -3N_{I,y} & 0\\ 0 & -N_{I,x} & 0\\ 0 & -N_{I,y} & 0\\ 0 & 4N_{I,x} & 0\\ 0 & 4N_{I,y} & 0\end{bmatrix};$$

$$\mathbf{B}_{1I}^{des}=\tfrac{1}{15}\begin{bmatrix}3N_{I,xx}+3N_{I,yy} & -3N_{I,xx}-3N_{I,yy} & 0\\ -4N_{I,xx}+N_{I,yy} & 4N_{I,xx}-N_{I,yy} & 0\\ -4N_{I,yy}+N_{I,xx} & 4N_{I,yy}-N_{I,xx} & 0\\ -5N_{I,xy} & 5N_{I,xy} & 0\end{bmatrix};$$

$$\mathbf{B}_{2I}^{des}=\frac{1}{15}\begin{bmatrix}0 & -6N_{I,xx}-6N_{I,yy} & 0\\ 0 & 8N_{I,xx}-2N_{I,yy} & 0\\ 0 & 8N_{I,yy}-2N_{I,xx} & 0\\ 0 & 10N_{I,xy} & 0\end{bmatrix};$$

$$\mathbf{B}_{rI}^{b1}=\tfrac{1}{4}\begin{bmatrix}4N_{I,xy} & 2N_{I,xy} & 0\\ -4N_{I,xy} & -2N_{I,xy} & 0\\ 2\left(N_{I,yy}-N_{Ixx}\right) & N_{I,yy}-N_{I,xx} & 0\end{bmatrix};$$

$$\mathbf{B}_{rI}^{b2}=\frac{1}{4}\begin{bmatrix}0 & -2N_{I,xy} & 0\\ 0 & 2N_{I,xy} & 0\\ 0 & N_{I,xx}-N_{I,yy} & 0\end{bmatrix};$$

$$\mathbf{B}_{1I}^{dil}=\begin{bmatrix}0 & 0 & 0\\ 0 & 0 & 0\\ -N_{I,xx}-N_{I,yy} & 0 & 0\end{bmatrix};$$

$$\mathbf{B}_{2I}^{dil}=\begin{bmatrix}-N_{I,xxx}-N_{I,xyy} & 0 & 0\\ -N_{I,yyy}-N_{I,xxy} & 0 & 0\\ 0 & 0 & 0\end{bmatrix};$$

$$\mathbf{B}_{3I}^{dil}=\begin{bmatrix}0 & N_{I,xxx}+N_{I,xyy} & 0\\ 0 & N_{I,yyy}+N_{I,xxy} & 0\\ 0 & 0 & 0\end{bmatrix};$$

$$\mathbf{B}_{4I}^{dil}=\begin{bmatrix}0 & 0 & 0\\ 0 & 0 & 0\\ 0 & N_{I,xx}+N_{I,yy} & 0\end{bmatrix}$$

Inserting Eq. (26) into Eq. (23), the vector $\mathbf{N_w}$ is reformed as

$$\mathbf{N_w}=\sum_{I=1}^{m\times n}\bar{\mathbf{B}}_{gI}\mathbf{q}_I;\ \bar{\mathbf{B}}_{gI}=\begin{bmatrix}N_{I,x} & N_{I,x} & 0\\ N_{I,y} & N_{I,y} & 0\end{bmatrix} \tag{30}$$

Besides, the displacement vector can be rewritten as

$$\bar{\mathbf{u}}=\begin{Bmatrix}\mathbf{u}_1\\ \mathbf{u}_2\\ \mathbf{u}_3\end{Bmatrix}=\sum_{I=1}^{m\times n}\begin{Bmatrix}\mathbf{N}_{1I}\\ \mathbf{N}_{2I}\\ \mathbf{N}_{3I}\end{Bmatrix}\mathbf{q}_I=\sum_{I=1}^{m\times n}\bar{\mathbf{N}}_I\mathbf{q}_I \tag{31}$$

where

$$\mathbf{N}_{1I}=\begin{bmatrix}0 & 0 & 0\\ 0 & 0 & 0\\ N_I & N_I & 0\end{bmatrix};\ \mathbf{N}_{2I}=\begin{bmatrix}-N_{I,x} & 0 & 0\\ -N_{I,y} & 0 & 0\\ 0 & 0 & 0\end{bmatrix};$$

$$\mathbf{N}_{3I}=\begin{bmatrix}0 & N_{I,x} & 0\\ 0 & N_{I,y} & 0\\ 0 & 0 & 0\end{bmatrix} \tag{32}$$

Substituting Eqs. (28), (30) and (31) into Eq. (24), the weak form for free vibration analysis of the FGPP microplate can be expressed as

$$\left(\mathbf{K}-\omega^2\mathbf{M}\right)\bar{\mathbf{q}}=0 \tag{33}$$

where ω and $\bar{q}$ are natural frequency and mode shapes, respectively; whereas $\mathbf{K}$ and $\mathbf{M}$ are the global stiffness matrix and mass matrix, respectively, defined as follows

$$\begin{aligned}\mathbf{K}=&\int_\Omega\bar{\mathbf{B}}_b^T\bar{\mathbf{D}}_{ub}\bar{\mathbf{B}}_b\mathrm{d}\Omega+\int_\Omega\bar{\mathbf{B}}_s^T\mathbf{D}_{us}\bar{\mathbf{B}}_s\mathrm{d}\Omega-\ldots\\ &\int_\Omega\bar{\mathbf{B}}_b^T\bar{\mathbf{D}}_{ueb}\bar{\mathbf{B}}_{eb}\mathrm{d}\Omega-\int_\Omega\bar{\mathbf{B}}_s^T\bar{\mathbf{D}}_{ues}\bar{\mathbf{B}}_{es}\mathrm{d}\Omega-\ldots\\ &\int_\Omega\bar{\mathbf{B}}_{eb}^T\bar{\mathbf{D}}_{ueb}^T\bar{\mathbf{B}}_b\mathrm{d}\Omega-\int_\Omega\bar{\mathbf{B}}_{es}^T\bar{\mathbf{D}}_{ues}^T\bar{\mathbf{B}}_s\mathrm{d}\Omega-\ldots\\ &\int_\Omega\bar{\mathbf{B}}_{eb}^T\bar{\mathbf{D}}_{eeb}\bar{\mathbf{B}}_{eb}\mathrm{d}\Omega-\int_\Omega\bar{\mathbf{B}}_{es}^T\bar{\mathbf{D}}_{ees}\bar{\mathbf{B}}_{es}\mathrm{d}\Omega+\ldots\\ &\int_\Omega\bar{\mathbf{B}}_{rb}^T\bar{\mathbf{D}}_{rb}\bar{\mathbf{\Gamma}}_{rb}\bar{\mathbf{B}}_{rb}\mathrm{d}\Omega+\int_\Omega\bar{\mathbf{B}}_{rs}^T\bar{\mathbf{D}}_{rs}\bar{\mathbf{\Gamma}}_{rs}\bar{\mathbf{B}}_{rs}\mathrm{d}\Omega+\ldots\\ &\int_\Omega\bar{\mathbf{B}}_{dil}^T\bar{\mathbf{D}}_{dil}\bar{\mathbf{B}}_{dil}\mathrm{d}\Omega+\int_\Omega\bar{\mathbf{B}}_{deb}^T\bar{\mathbf{D}}_{deb}\bar{\mathbf{\Gamma}}_{deb}\bar{\mathbf{B}}_{deb}\mathrm{d}\Omega+\ldots\\ &\int_\Omega\bar{\mathbf{B}}_{des}^T\bar{\mathbf{D}}_{des}\bar{\mathbf{\Gamma}}_{des}\bar{\mathbf{B}}_{des}\mathrm{d}\Omega-\int_\Omega\bar{\mathbf{B}}_g^T\mathbf{N}_e\bar{\mathbf{B}}_g\mathrm{d}\Omega;\end{aligned} \tag{34}$$

$$\mathbf{M}=\int_\Omega\bar{\mathbf{N}}^T\bar{\mathbf{m}}\bar{\mathbf{N}}\mathrm{d}\Omega;\ \mathbf{q}=\bar{\mathbf{q}}\mathrm{e}^{i\omega t}$$

3. Numerical Results

Firstly, we consider a FGP square plate with the material properties given in Ref. [32] to verify the accuracy and accord of the proposed model. The boundary conditions combine with clamped (C) and simply supported (S) edges. Table 1 shows the natural frequency $\bar{\omega}=\omega a^2\sqrt{\rho_c/E_c}/h$ of the FGP square plates with various external electric voltages and BCs. As we see in Tab. 1, the numerical results of the presented method match very well with those given by Su et al. [32]. The comparison results in Tab. 1 show that the proposed model is accurate and in accord.

Next, a FGPP rectangular microplate with the material properties shown in Tab. 2 is investigated. For numerical investigation of the problem, the three LSPs are taken the same ($l_1=l_2=l_3=l$) [15]. The effect of the porosity coefficient and scale-to-thickness ratio (l/h) on the dimensional natural frequency $\widehat{\omega}=\omega a^2\sqrt{\rho_1/c_{111}}/h$ of the FGPP square microplate with various porous distributions is tabulated in Tab. 3. It can be seen that from Tab. 3, a

rise of the porosity coefficient and LSPs makes a decrease and increase of the first dimensionless natural frequency of the FGPP microplates, respectively. Table 4 presents the first dimensionless natural frequency of the FGPP square microplates with various external electric voltages. We can see in Tab. 4 that the natural frequency of the FGPP microplate decreases with an increase of the electric voltage. Finally, the influence of the length-to-thickness and width-to-length ratios on the first dimensionless natural frequencies of the SSSS FGPP rectangular microplates is listed in Tab. 5. The frequency of the microplate increases and decreases with a rise of the length-to-thickness ratio and the width-to-length ratio, respectively.

Furthermore, the free vibration of the FGPP circular microplates with radius R and thickness h is investigated. Table 6 presents the influence of the LSPs and porosity coefficient on the first dimensionless natural frequency $\tilde{\omega} = \omega R^2 \sqrt{\rho_1 / c_{111}} / h$ of the FGPP circular microplates. It can be observed that from Tab. 6, a rise of the scale-to-thickness ratio and porosity coefficient makes a rise and a decrease of the natural frequency of the FGPP microplates, respectively. Besides, the first five non-dimensional natural frequenciesof $\tilde{\omega}$ the FGPP circular microplates with various radius-to-thickness ratios and external electric voltages are tabulated in Tab. 7 and Tab. 8, respectively. As we see in Tab. 7 and Tab. 8, an increase of the radius-to-thickness ratio and external electric voltage leads to the growth and decrease the frequency of the microplates.

4. Conclusion

In this paper, the size-dependent free vibration of the FGPP microplates with various porous distributions, including uniform and non-uniform distributions under the external electric load was first studied based on the RPT with two variables, MSGT and IGA. The accuracy and accord of the proposed method have been verified through comparisons with previous references. The influence of the LSPs, porosity distributions, porous coefficient and geometries on the natural frequency of the FGPP rectangular and circular microplates was investigated in detail. The results show that a rise in the LSPs and length-to-thickness ratio leads to an increase in the stiffness of the microplate, while a rise in the porous coefficient, electric voltage and width-to-length ratio makes a decrease in the microplate's stiffness. The numerical results of the proposed model can be considered benchmark results for further studies of FGPP microstructures.

References

[1] Huang, X.L. & Shen, H.S. (2006). Vibration and dynamic response of functionally graded plates with piezoelectric actuators in thermal environments. *Journal of Sound and Vibration*, *289*(1-2), 25–53.

[2] Ebrahimi, F., Rastgoo, A., & Bahrami, M.N. (2010). Investigating the thermal environment effects on geometrically nonlinear vibration of smart functionally graded plates. *Journal of mechanical science and technology*, *24*(3), 775–791.

[3] Yan, Z. & Jiang, L. (2012). Vibration and buckling analysis of a piezoelectric nanoplate considering surface effects and in-plane constraints. *Proceedings of the Royal Society A: Mathematical, Physical and Engineering Sciences*, *468*(2147), 3458–3475.

[4] Ebrahimi, F. (2013). Analytical investigation on vibrations and dynamic response of functionally graded plate integrated with piezoelectric layers in thermal environment. *Mechanics of Advanced Materials and Structures*, *20*(10), 854–870.

[5] Arani, A.G., Kolahchi, R., & Esmailpour, M. (2016). Nonlinear vibration analysis of piezoelectric plates reinforced with carbon nanotubes using DQM. *Smart Struct Syst, Int J*, *18*(4), 787–800.

[6] Duc, N.D., Cong, P.H., & Quang, V.D. (2016). Nonlinear dynamic and vibration analysis of piezoelectric eccentrically stiffened FGM plates in thermal environment. *International Journal of Mechanical Sciences*, *115*, 711–722.

Tab. 1: The nondimensional vibration frequency of the SSSS FG piezoelectric square plates with ($a/h = 100$, $l = 0$).

BCs	$V_0(V)$	$p = 0.1$		$p = 1$		$p = 2$		$p = 6$	
		Ref. [32]	Present	Ref. [32]	Present	Ref. [32]	Present	Ref. [32]	Present
CCCC	-200	9.483	9.490	9.083	9.088	8.988	8.987	8.865	8.853
	0	9.426	9.433	9.011	9.016	8.910	8.909	8.780	8.768
	200	9.369	9.376	8.938	8.944	8.831	8.831	8.694	8.681
CFCF	-200	5.721	5.744	5.475	5.502	5.417	5.441	5.342	5.360
	0	5.699	5.693	5.410	5.437	5.346	5.371	5.264	5.282
	200	5.617	5.641	5.343	5.372	5.273	5.300	5.185	5.204
SCSC	-200	7.670	7.673	7.354	7.355	7.280	7.277	7.184	7.172
	0	7.606	7.609	7.272	7.274	7.192	7.188	7.088	7.075
	200	7.540	7.544	7.190	7.192	7.102	7.099	6.989	6.977
CCFF	-200	1.796	1.800	1.743	1.748	1.733	1.738	1.720	1.723
	0	1.695	1.699	1.616	1.622	1.596	1.602	1.571	1.574
	200	1.586	1.591	1.474	1.482	1.441	1.449	1.400	1.405

Tab. 2: The material properties of the FGPP microplate.

Properties	Pzt-4
Elastic (GPa)	$c_{11} = c_{22} = 138.499$; $c_{12} = 77.371$; $c_{13} = 73.643$; $c_{33} = 114.745$; $c_{55} = 25.6$; $c_{66} = 30.6$
Piezoelectric constant (Cm^{-2})	$e_{31} = -5.2$; $e_{33} = 15.08$; $e_{15} = 12.72$
Dielectric constant (10^{-9} $\mathrm{C}^2\mathrm{m}^{-2}\mathrm{N}^{-1}$)	$k_{11} = 1.306$; $k_{33} = 1.115$
Density (kgm^{-3})	7600

Tab. 3: The first dimensionless natural frequency of the FGPP square microplates with various scale-to-thickness ratios and porosity coefficients ($a/h = 10$, $V_0 = 0$).

Type	BCs	e_0	l/h				
			0	0.1	0.2	0.5	1
Uniform	SSSS	0.1	5.8628	6.0684	6.6466	9.7759	16.7027
		0.2	5.7572	5.9591	6.5269	9.5998	16.4018
		0.3	5.6426	5.8404	6.3969	9.4086	16.0752
	SFSF	0.1	2.5572	2.6937	3.0520	4.7542	8.2705
		0.2	2.5111	2.6451	2.9970	4.6685	8.1215
		0.3	2.4611	2.5925	2.9373	4.5756	7.9598
	SCSC	0.1	8.1076	8.4221	9.2947	13.8979	23.9276
		0.2	7.9616	8.2704	9.1273	13.6475	23.4965
		0.3	7.8030	8.1057	8.9455	13.3758	23.0286
	CCCC	0.1	9.7343	10.1256	11.2063	16.8549	29.0911
		0.2	9.5589	9.9431	11.0044	16.5512	28.5670
		0.3	9.3686	9.7452	10.7853	16.2217	27.9982
Non-uniform	SSSS	0.1	5.9367	6.1405	6.7146	9.8340	16.7635
		0.2	5.9148	6.1135	6.6738	9.7294	16.5415
		0.3	5.8961	6.0899	6.6369	9.6274	16.3179
	SFSF	0.1	2.5928	2.7276	3.0827	4.7785	8.2939
		0.2	2.5874	2.7181	3.0636	4.7233	8.1767
		0.3	2.5843	2.7109	3.0464	4.6688	8.0583
	SCSC	0.1	8.1992	8.5125	9.3830	13.9886	24.0490
		0.2	8.1558	8.4633	9.3179	13.8487	23.7678
		0.3	8.1134	8.4161	9.2566	13.7135	23.4874
	CCCC	0.1	9.8307	10.2222	11.3040	16.9705	29.2670
		0.2	9.7625	10.1486	11.2155	16.8071	28.9559
		0.3	9.6921	10.0745	11.1296	16.6499	28.6484

Tab. 4: The first dimensionless natural frequency of the FGPP square microplates with various external electric voltages and porous distribution ($a/h = 50$, $e_0 = 0.1$, $l/h = 0.2$).

Type	$V_0(V)$	BCs				
		SSSS	SFSF	SCSC	CCCC	CCFF
Uniform	-500	6.8765	3.1220	9.9616	12.3211	2.2024
	0	6.8579	3.1000	9.9474	12.3086	2.1790
	500	6.8392	3.0779	9.9332	12.2961	2.1553
Non-uniform	-500	6.9561	3.1549	10.0761	12.4620	2.2255
	0	6.9376	3.1331	10.0621	12.4497	2.2024
	500	6.9191	3.1112	10.0480	12.4373	2.1789

Tab. 5: The influence of the width-to-length ratio and length-to-thickness ratio on the natural frequency of the SSSS FGPP rectangular microplates ($e_0 = 0.4$, $l/h = 0.4$, $V_0 = 0$).

Type	b/a	a/h				
		10	20	30	40	50
Uniform	1	8.0700	8.2707	8.3108	8.3251	8.3317
	1.5	5.8839	5.9888	6.0093	6.0165	6.0199
	2	5.1090	5.1873	5.2024	5.2078	5.2102
Non-uniform	1	8.4039	8.6178	8.6604	8.6756	8.6826
	1.5	6.1293	6.2406	6.2623	6.2699	6.2735
	2	5.3226	5.4055	5.4215	5.4271	5.4298

Tab. 6: The first dimensionless natural frequency of the FGPP circular microplates with various scale-to-thickness ratios and porosity coefficients ($R = 1$, $R/h = 10$, $V_0 = 0$).

Type	BCs	e_0	l/h				
			0	0.1	0.2	0.5	1
Uniform	SSSS	0.1	1.6318	1.6795	1.8146	2.5636	4.2704
		0.2	1.6024	1.6493	1.7819	2.5174	4.1935
		0.3	1.5705	1.6164	1.7464	2.4673	4.1100
	CCCC	0.1	2.9724	3.0864	3.4005	5.0617	8.6963
		0.2	2.9188	3.0308	3.3392	4.9705	8.5396
		0.3	2.8607	2.9705	3.2728	4.8715	8.3696
Non-uniform	SSSS	0.1	1.6553	1.7024	1.8360	2.5799	4.2826
		0.2	1.6526	1.6983	1.8280	2.5536	4.2223
		0.3	1.6516	1.6958	1.8216	2.5281	4.1615
	CCCC	0.1	3.0122	3.1254	3.4372	5.0921	8.7266
		0.2	3.0039	3.1142	3.4184	5.0384	8.6095
		0.3	2.9976	3.1053	3.4020	4.9862	8.4916

Tab. 7: The first five dimensionless natural frequencies of the FGPP circular microplates with various radius-to-thickness ratios ($R = 1$, $e_0 = 0.4$, $l/h = 0.3$, $V_0 = 0$).

Type	BCs	R/h	Mode				
			1	2	3	4	5
Uniform	SSSS	5	1.8551	4.8014	4.8203	8.3556	8.3574
		10	1.8997	5.0979	5.1044	9.1651	9.1664
		15	1.9087	5.1648	5.1679	9.3707	9.3718
		20	1.9119	5.1893	5.1911	9.4487	9.4498
	CCCC	5	3.3767	6.6823	6.7299	10.4954	10.5203
		10	3.6352	7.4295	7.4500	11.9710	11.9820
		15	3.6979	7.6289	7.6393	12.4036	12.4098
		20	3.7218	7.7066	7.7128	12.5704	12.5878
Non-uniform	SSSS	5	1.9499	5.0043	5.0308	8.6618	8.6621
			2.0032	5.3534	5.3625	9.6016	9.6025
			2.0139	5.4328	5.4371	9.8430	9.8439
			2.0177	5.4619	5.4644	9.9350	9.9359
	CCCC	5	3.5285	6.9356	6.9996	10.8483	10.8639
		10	3.8173	7.7825	7.8101	12.5201	12.5231
		15	3.8870	8.0095	8.0236	13.0061	13.0198
		20	3.9135	8.0979	8.1063	13.1980	13.2223

Tab. 8: The effect of the external electric voltage on the first five dimensionless natural frequencies of the FGPP circular microplates ($R = 1$, $R/h = 50$, $e_0 = 0.1$, $l/h = 0.2$).

Type	BCs	$V_0(V)$	Mode				
			1	2	3	4	5
Uniform	SSSS	-500	1.8499	4.9492	4.9493	9.0096	9.0103
		0	1.8295	4.9299	4.9300	8.9905	8.9913
		500	1.8088	4.9105	4.9106	8.9715	8.9722
	CCCC	-500	3.5295	7.3282	7.3287	11.9822	12.0275
		0	3.5168	7.3134	7.3140	11.9664	12.0117
		500	3.5041	7.2986	7.2992	11.9506	11.9959
Non-uniform	SSSS	-500	1.8719	5.0071	5.0073	9.1145	9.1152
		0	1.8517	4.9880	4.9882	9.0956	9.0964
		500	1.8312	4.9689	4.9690	9.0768	9.0776
	CCCC	-500	3.5701	7.4126	7.4132	12.1195	12.1659
		0	3.5576	7.3980	7.3985	12.1038	12.1503
		500	3.5450	7.3833	7.3839	12.0882	12.1347

[7] Ellali, M., Amara, K., Bouazza, M., & Bourada, F. (2018). The buckling of piezoelectric plates on pasternak elastic foundation using higher-order shear deformation plate theories. *Smart structures and systems*, *21*(1), 113–122.

[8] Tanzadeh, H. & Amoushahi, H. (2019). Buckling and free vibration analysis of piezoelectric laminated composite plates using various plate deformation theories. *European Journal of Mechanics-A/Solids*, *74*, 242–256.

[9] El Harti, K., Rahmoune, M., Sanbi, M., Saadani, R., Bentaleb, M., & Rahmoune, M. (2019). Vibrations piezo-control of FGM beam in a thermal environment. In *MATEC Web of Conferences*, volume 286, EDP Sciences, 01001.

[10] Liu, T., Jiang, Y., Li, S., Liu, Q., & Wang, C. (2021). Isogeometric Analysis for Active Control of Piezoelectric Functionally

Graded Plates in Thermal Environment. *Shock and Vibration*, *2021*.

[11] Phuc, P.M. & Kim Khue, N.T. (2021). New finite modeling of free and forced vibration responses of piezoelectric FG plates resting on elastic foundations in thermal environments. *Shock and Vibration*, *2021*.

[12] Ahmed, R.A., Khalaf, B.S., Raheef, K.M., Fenjan, R.M., & Faleh, N.M. (2021). Investigating dynamic response of nonlocal functionally graded porous piezoelectric plates in thermal environment. *Steel Compos Struct*, *40*(2), 243–254.

[13] Abbaspour, F. & Arvin, H. (2021). Vibration analysis of piezoelectric graphene platelets micro-plates. *AUT Journal of Mechanical Engineering*, *5*(3), 2–2.

[14] Wang, W., Li, H., & Yao, L. (2022). Static Bending and Vibration Analysis of a Rectangular Functionally Gradient Piezoelectric Plate on an Elastic Foundation. *Applied Sciences*, *12*(3), 1517.

[15] Lam, D.C., Yang, F., Chong, A., Wang, J., & Tong, P. (2003). Experiments and theory in strain gradient elasticity. *Journal of the Mechanics and Physics of Solids*, *51*(8), 1477–1508.

[16] Li, Y. & Feng, W. (2014). Microstructure-dependent piezoelectric beam based on modified strain gradient theory. *Smart materials and structures*, *23*(9), 095004.

[17] Mohammadi, M., Fooladi, M., & Darijani, H. (2015). Exact boundary conditions for buckling analysis of rectangular microplates based on the modified strain gradient theory. *International Journal for Multiscale Computational Engineering*, *13*(3).

[18] Ashoori, A. & Mahmoodi, M. (2015). The modified version of strain gradient and couple stress theories in general curvilinear coordinates. *European Journal of Mechanics-A/Solids*, *49*, 441–454.

[19] Hosseini, M., Bahreman, M., & Jamalpoor, A. (2016). Using the modified strain gradient theory to investigate the size-dependent biaxial buckling analysis of an orthotropic multi-microplate system. *Acta Mechanica*, *227*(6), 1621–1643.

[20] Kandaz, M. & Dal, H. (2018). A comparative study of modified strain gradient theory and modified couple stress theory for gold microbeams. *Archive of Applied Mechanics*, *88*(11), 2051–2070.

[21] Karamanli, A. & Vo, T.P. (2021). A quasi-3D theory for functionally graded porous microbeams based on the modified strain gradient theory. *Composite Structures*, *257*, 113066.

[22] Hughes, T.J., Cottrell, J.A., & Bazilevs, Y. (2005). Isogeometric analysis: CAD, finite elements, NURBS, exact geometry and mesh refinement. *Computer methods in applied mechanics and engineering*, *194*(39-41), 4135–4195.

[23] Bazilevs, Y., Takizawa, K., Tezduyar, T.E., Hsu, M.C., Otoguro, Y., Mochizuki, H., & Wu, M.C. (2020). Wind turbine and turbomachinery computational analysis with the ALE and space-time variational multiscale methods and isogeometric discretization. *Journal of Advanced Engineering and Computation*, *4*(1).

[24] Takizawa, K., Bazilevs, Y., Tezduyar, T.E., Hsu, M.C., & Terahara, T. (2022). Computational cardiovascular medicine with isogeometric analysis. *Journal of Advanced Engineering and Computation*, *6*(3), 167–199.

[25] Takizawa, K., Bazilevs, Y., E Tezduyar, T., & Hsu, M.C. (2019). Computational cardiovascular flow analysis with the variational multiscale methods. *Journal of Advanced Engineering and Computation*, *3*(2).

[26] Takizawa, K., Bazilevs, Y., & Tezduyar, T.E. (2022). Mesh moving methods in flow computations with the space-time and arbitrary Lagrangian-Eulerian methods. *Journal of Advanced Engineering and Computation*, *6*(2), 85–112.

[27] Thai, C.H., Ferreira, A., & Nguyen-Xuan, H. (2018). Isogeometric analysis of size-dependent isotropic and sandwich functionally graded microplates based on modified

strain gradient elasticity theory. *Composite Structures*, *192*, 274–288.

[28] Thai, C.H., Ferreira, A., & Phung-Van, P. (2019). Size dependent free vibration analysis of multilayer functionally graded GPLRC microplates based on modified strain gradient theory. *Composites Part B: Engineering*, *169*, 174–188.

[29] Thai, C.H., Ferreira, A., Rabczuk, T., & Nguyen-Xuan, H. (2018). Size-dependent analysis of FG-CNTRC microplates based on modified strain gradient elasticity theory. *European Journal of Mechanics-A/Solids*, *72*, 521–538.

[30] Shimpi, R.P. (2002). Refined plate theory and its variants. *AIAA journal*, *40*(1), 137–146.

[31] Ke, L.L., Wang, Y.S., Yang, J., & Kitipornchai, S. (2014). Free vibration of size-dependent magneto-electro-elastic nanoplates based on the nonlocal theory. *Acta Mechanica Sinica*, *30*(4), 516–525.

[32] Su, Z., Jin, G., & Ye, T. (2018). Electro-mechanical vibration characteristics of functionally graded piezoelectric plates with general boundary conditions. *International Journal of Mechanical Sciences*, *138*, 42–53.

About Authors

P. T. HUNG was born in Vietnam in 1981. He has a Ph.D. degree in Mechanics. Now, he is a lecturer at the Faculty of Civil Engineering at Ho Chi Minh City University of Technology and Education, Ho Chi Minh City, Vietnam. His research interests are computational mechanics.

P. PHUNG-VAN received his Ph.D from Ghent University in 2016. He has been conducting computational mechanics research since 2012. Currently, he is a senior lecturer at the Faculty of Civil Engineering, HUTECH University, Ho Chi Minh City, Vietnam. He has published over 58 Web-of-Science-indexed journal articles on computational and structural mechanics and nanostructures. He is one of World's Best Mechanical and Aerospace Engineering Scientists according to Research.com. He is also one of the Best Rising Stars of Science in the World - 2022.